Electronic properties of zircon and hafnon from many-body perturbation theory

R. Shaltaf, T. Rangel, M. Grüning, X. Gonze, and G.-M. Rignanese
Unité de Physico-Chimie et de Physique des Matériaux (PCPM), European Theoretical Spectroscopy Facility (ETSF), Université catholique de Louvain, 1 Place Croix du Sud, B-1348 Louvain-la-Neuve, Belgium

D. R. Hamann
Department of Physics and Astronomy, Rutgers University, Piscataway, New Jersey 08854-8019, USA and Mat-Sim Research LLC, P.O. Box 742, Murray Hill, New Jersey 07974, USA

(Received 22 December 2008; revised manuscript received 2 April 2009; published 1 May 2009)

The electronic properties of zircon and hafnon, two wide-gap high-κ materials, are investigated using many-body perturbation theory (MBPT) combined with the Wannier interpolation technique. For both materials, the calculated band structures differ from those obtained within density-functional theory and MBPT by (i) a slight displacement of the highest valence-band maximum from the Γ point and (ii) an opening of the indirect band gap to 7.6 and 8.0 eV for zircon and hafnon, respectively. The introduction of vertex corrections in the many-body self-energy does not modify the results except for a global rigid shift of the many-body corrections.

DOI: 10.1103/PhysRevB.79.195101 PACS number(s): 71.15.Ap, 71.20.−b

I. INTRODUCTION

Zircon ($ZrSiO_4$) and hafnon ($HfSiO_4$) are materials of technological relevance. Due to their durability and ability to host large quantities of long-lived actinides, they are used for nuclear waste disposal.[1] On the other hand, they both possess high dielectric constants and large energy gaps which made them emerge as high-κ gate dielectric materials in metal-oxide-semiconductor technology.[2–5]

Due to the similarity of the physical and chemical properties of Zr and Hf, the structural and electronic properties of zircon and hafnon are very much alike. At ambient conditions, they present a body-centered tetragonal crystal structure (space group $I41/amd$, No. 141) with 2 f.u. $MSiO_4$ (M=Hf,Zr) in the primitive cell. In this structure, each M =(Hf,Zr) atom is bonded to eight O atoms, while each Si atom is bonded to four O atoms so that each O atom is bonded to two M=(Hf,Zr) and one Si atoms. At higher pressure, zircon and hafnon stabilize in a scheelite structure (space group $I_{4_1/a}$, No. 88), with a Bravais lattice which is also body-centered tetragonal with the same number of atoms as in the low-pressure phase.

Various properties of hafnon and zircon have been investigated within density-functional theory (DFT): pressure-induced phase-transition,[6,7] properties of point defects,[8–10] dynamical, electronic, and dielectric properties.[11–13] In these studies, DFT proved to be successful in reproducing many experimental results. However, it is well known that DFT fails to give a reliable estimation of the electronic energy gap[14,15] Such an excited-state property can be accessed directly through the many-body perturbation theory (MBPT) formalism.[16] Today MBPT is considered a reliable and well-established method for electronic band-structure calculations, which makes it an ideal choice for energy gap prediction when little experimental information is available.

Experimentally, a direct measure of the energy gap of zircon and hafnon in their crystalline phase is still missing.[10,17] In practice, the value of 6.5–7.0 eV, which has been extrapolated from measurements on $(MO_2)_x(SiO_2)_y$ disordered alloys grown on Si,[18–20] is often considered as the reference.[2,10,17] This can be reasonably questioned given the structural difference between amorphous alloys and single-crystal phases. On the other hand, values ranging from 5.0 to 7.7 eV have been reported for the Kohn-Sham energy gap, as calculated within the local-density approximation (LDA) (Refs. 11 and 12) and weighted density approximation (WDA).[10,17] However, these values are subject to the above-mentioned criticisms and cannot be considered as reliable.

The aim of this work is to provide a more accurate prediction of the energy band gap of zircon and hafnon based on MBPT. The precise knowledge of energy band gap and the associated many-body corrections with respect to the standard DFT approach is crucial for band-offset calculations.[10,21] Our results will hopefully reduce the uncertainty present in the literature. The paper is organized as follows. In Sec. II, we briefly present the *GW* method and the interpolation scheme, based on Wannier functions, allowing for a full MBPT band structure to be obtained. In Sec. III, we detail the numerical parameters of the calculations. In Sec. IV, we present and discuss the band structure obtained within DFT-LDA and *GW* approximations.

II. THEORETICAL BACKGROUND

Within MBPT, the quasiparticle eigenfunctions and eigenenergies are calculated by solving the Dyson equation:[22–24]

$$\left(-\frac{1}{2}\nabla^2 + V^{\text{ext}} + V^H\right)\psi_{n\mathbf{k}} + \int \Sigma(\mathbf{r},\mathbf{r}',\omega=\epsilon_{n\mathbf{k}})\psi_{n\mathbf{k}}d^3\mathbf{r} = \epsilon_{n\mathbf{k}}\psi_{n\mathbf{k}}, \quad (1)$$

where V^{ext} stands for the crystal external potential, V^H is the Hartree potential, and Σ is the nonlocal energy-dependent self-energy operator. Σ can be evaluated by solving Hedin equations[22] starting from the Hartree approximation, i.e., ne-

glecting exchange and correlation effects. This leads to the so-called *GW* approximation:

$$\Sigma(\mathbf{r},\mathbf{r}',\omega) = \frac{i}{2\pi}\int d\omega' e^{i\omega'\eta} G(\mathbf{r},\mathbf{r}',\omega+\omega')W(\mathbf{r},\mathbf{r}',\omega'), \tag{2}$$

where G and W are the single-particle Green's function and the screened Coulomb interaction, respectively. Alternatively, the Hedin equations can be solved taking into account further exchange and correlation effects known as vertex corrections, leading to the so-called $GW\Gamma$ approximation.[25]

In principle, Eq. (1) should be solved self-consistently to obtain the quasiparticle eigenenergies and eigenfunctions. However, the standard approach is to use the Kohn-Sham wave functions ($\psi_{n\mathbf{k}}^{\mathrm{DFT}}$) and eigenenergies ($\epsilon_{n\mathbf{k}}^{\mathrm{DFT}}$) as a zero-order approximation for their quasiparticle counterparts and proceed within first-order perturbation theory:

$$\epsilon_{n\mathbf{k}} = \epsilon_{n\mathbf{k}}^{\mathrm{DFT}} + \bar{\Sigma}_{n\mathbf{k}}, \tag{3}$$

where $\bar{\Sigma}_{n,k}$ is the quasiparticle correction given by

$$\bar{\Sigma}_{n\mathbf{k}} = \mathrm{Re}\left\{\frac{1}{Z}\langle\psi_{n\mathbf{k}}^{\mathrm{DFT}}|\Sigma(\omega=\epsilon_{n\mathbf{k}}^{\mathrm{DFT}}) - V_{\mathrm{xc}}|\psi_{n\mathbf{k}}^{\mathrm{DFT}}\rangle\right\}, \tag{4}$$

and Z is a normalization factor,

$$Z = \left[1 - \frac{\partial\Sigma}{\partial\omega}\bigg|_{\omega=\epsilon_{n\mathbf{k}}^{\mathrm{DFT}}}\right]^{-1}. \tag{5}$$

The knowledge of W over a wide range of frequencies is required to evaluate the frequency convolution in Eq. (2). However, the integral can be handled by modeling the dynamic dependence of W using the single plasmon pole model (PPM) approximation. The advantage is not only a significant reduction in the computational cost but also the ability to evaluate the self-energy analytically. In this work, the PPM proposed by Godby and Needs[26] is used. This model is formally identical to the one previously proposed by Hybertsen and Louie.[23] However, the PPM parameters are obtained from the computation of the screening matrix at an imaginary frequency (typically the plasmon frequency), where the inverse dielectric matrix is well behaved. The choice of this model with respect to other models proposed in the literature is motivated by the recent finding that it gives the best agreement with explicit numerical integration results.[21]

The exact evaluation of the *GW* correction, for a full band structure along different symmetry lines in the Brillouin zone (BZ) via Eq. (3), can be an extremely demanding task. In the literature, it is quite standard to compute the *GW* corrections for several special **k** points, and then to deduce a scissor correction, i.e., a constant shift to be applied to conduction-band DFT eigenvalues, to be used for the less-symmetric **k** points. A more refined procedure involves linear interpolation of the eigenenergies between the available **k** points.

Another more convenient approach is to interpolate the many-body corrections using a scheme based on maximally localized Wannier functions (MLWFs).[27] This approach has already been used in band-structure interpolation.[28,29] Its advantage over other existing schemes comes from the fact that it preserves valuable information about band connectivity. Hence, band crossings, avoided crossings, and degeneracies are treated correctly.

The MLWFs can be constructed from a set of Bloch eigenstates $\psi_{n\mathbf{k}}$:

$$|\mathcal{W}_{m\mathbf{R}}\rangle = \frac{V}{(2\pi)^3}\int_{\mathrm{BZ}}\sum_{n=1}^{N} U_{nm}^{(\mathbf{k})}|\psi_{n\mathbf{k}}\rangle e^{-i\mathbf{k}\cdot\mathbf{R}}d\mathbf{k}. \tag{6}$$

Here $\mathcal{W}_{m\mathbf{R}}$ is the mth Wannier wave function at the unit cell vector $\mathbf{R}$; $U_{nm}^{(\mathbf{k})}$ are unitary matrices with dimension N that generates an N-dimensional manifold of Bloch states $\psi_{n\mathbf{k}}$. The choice of manifold dimensions is natural in systems where the energy bands appear as isolated groups separated from each other by energy gaps. However, in cases where the bands of interest are not isolated, an additional disentangling procedure is needed.[30] $U_{nm}^{(\mathbf{k})}$ is chosen, within the maximally localized Wannier function scheme, in such a way that the quadratic extent of wave functions is minimized.[27]

Following the description of Refs. 28 and 29, given a set of quasiparticle eigenvalues, $\epsilon_{n\mathbf{k}}$ (be it the DFT-LDA or the *GW* ones), calculated on a homogeneous **k**-point grid, the unitary transformation matrices $U_{nm}^{(\mathbf{k})}$ can be used to calculate the matrix elements in the Wannier gauge representation:

$$H_{nm\mathbf{k}}^{\mathcal{W}} = [(U^{(\mathbf{k})})^{\dagger}HU^{(\mathbf{k})}]_{nm}, \tag{7}$$

where $H_{nm\mathbf{k}} = \epsilon_{n\mathbf{k}}\delta_{nm}$.

We then calculate the matrix elements in real space using Fourier transform:

$$H_{nm\mathbf{R}}^{\mathcal{W}} = \frac{1}{N_k}\sum_{\mathbf{k}} \exp^{-i\mathbf{k}\cdot R}H_{nm\mathbf{k}}^{\mathcal{W}}. \tag{8}$$

Then assuming that $|H_{nm\mathbf{R}}^{\mathcal{W}}|$ to decay fast with $|\mathbf{R}|$, we can recover the matrix elements at any arbitrary $\mathbf{k}'$ point over BZ (even if such **k** point is not part of the original special **k** points list) using direct sum over all lattice vectors **R** in the supercell conjugate to the **k** mesh:

$$H_{nm\mathbf{k}'}^{\mathcal{W}} = \sum_{\mathbf{R}} e^{i\mathbf{k}'\cdot R}H_{nm\mathbf{R}}^{\mathcal{W}}. \tag{9}$$

The final step is to transform back from the Wannier gauge to get $\epsilon_{n\mathbf{k}'}$ by finding the suitable unitary transformation $U^{(\mathbf{k}')}$. This can be achieved by simple diagonalization of $H_{nm\mathbf{k}'}^{\mathcal{W}}$. Note that a similar procedure can also be applied to interpolate the quasiparticle corrections $\bar{\Sigma}_{n\mathbf{k}}$. The above procedure is a convenient method which allows the calculation of a full band structure within *GW* approximation using a limited **k**-point grid without encountering the drawbacks that would arise using the linear interpolation method (e.g., difficulties to treat correctly the band crossings).

III. TECHNICAL DETAILS

All the ground-state and *GW* calculations are performed using the ABINIT code.[31] The ion-electron interaction is approximated by highly transferable extended norm-conserving

pseudopotentials.[32] The pseudopotentials are constructed considering the following states as valence ones: Hf($5s,5p,5d,6s$), Zr($4s,4p,4d,5s$), Si($3s,3p$), and O($2s,2p$). The wave functions are expanded onto a plane-wave basis setup to a kinetic energy cutoff of 30 hartree. The Brillouin-zone integration is performed using a special $4\times4\times4$ wave vector grid sampled within the Monkhorst-Pack scheme.[33] The dielectric matrix is calculated using the Adler-Wiser expression[34] summing over 300 bands. We find that using a matrix size of 345×345 plane waves to represent the dielectric matrix is enough to account for inclusion of local field effects and to achieve convergence of quasiparticle energies. The self-energy Σ is obtained by summing over 24 special $\mathbf{q}$ vectors in the irreducible BZ, and over 400 bands. For $GW\Gamma$ calculations, approximate vertex corrections have been included following the method proposed in Ref. 25. For both GW and $GW\Gamma$ approaches, the calculations are repeated iteratively by correcting the unoccupied eigenvalues with a scissor operator matching the quasiparticle gap from one iteration to construct the Green's functions for the next iteration until convergence of the quasiparticle gap is reached.[35] Such procedures are referred to as GW_0 and $GW_0\Gamma$.

All the calculations are performed with the low-pressure body-centered tetragonal structure. In this structure, both M =(Hf,Zr) and Si atoms are located at high-symmetry positions $(0,\frac{3}{8},\frac{1}{4})$ and $(0,\frac{1}{4},\frac{3}{8})$ on the $4a$ and $4b$ Wyckoff sites, respectively. The O atoms occupy the $16h$ Wyckoff sites at $(0,u,v)$, where u and v are internal parameters. The theoretical parameters used throughout all the calculations are identical to those reported in Ref. 12.

IV. RESULTS

Starting from the set of DFT-LDA eigenvalues and eigenfunctions calculated on the $\mathbf{k}$-points grid, the quasiparticle corrections are computed for the same set of $\mathbf{k}$-points following Eqs. (3)–(5). Then, the quasiparticle corrections are interpolated for the high-symmetry segments of the BZ using MLWFs as described in Sec. II. In order for Eq. (9) to be really advantageous, the real-space representation $|H^{\mathcal{W}}_{nm\mathbf{R}}|$ of the DFT-LDA and GW Hamiltonians need to have a sufficiently fast decay with $|\mathbf{R}|$. In principle, this decay should be monitored for each pair of n and m indices individually. Alternatively, a global view on the decay can be obtained by summing the square of the matrix elements for the group of bands under consideration:

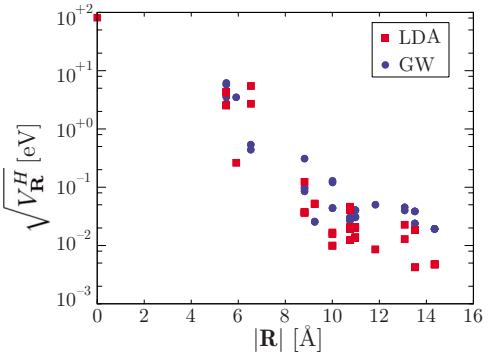

FIG. 1. (Color online) Global decay of the real-space representation of the DFT-LDA (blue circles) and GW (red squares) Hamiltonians as a function of the lattice vector size $|\mathbf{R}|$ are measured by $\sqrt{V^H_{\mathbf{R}}}$ [see Eq. (10)] for all the valence bands.

$$V^H_{\mathbf{R}} = \sum_{n,m} |H^{\mathcal{W}}_{nm\mathbf{R}}|^2 = \sum_{n,m} |\langle \mathcal{W}_{n\mathbf{R}}|H|\mathcal{W}_{m0}\rangle|^2, \tag{10}$$

and taking the square root of this sum. Interestingly, it can be shown that $V^H_{\mathbf{R}}$ is nothing but $\mathrm{Tr}[HP_{\mathbf{R}}HP_0]$, where $P_{\mathbf{R}}$ is the projection operator onto the corresponding group of Wannier functions attached to the vector $\mathbf{R}$:

$$P_{\mathbf{R}} = \sum_n |\mathcal{W}_{n\mathbf{R}}\rangle\langle\mathcal{W}_{n\mathbf{R}}|. \tag{11}$$

As illustrated in Fig. 1, $\sqrt{V^H_{\mathbf{R}}}$ decays exponentially showing that the $\mathbf{k}$-points grid used in the Wannier interpolation is indeed sufficient.

The GW_0 band structure along the high-symmetry lines of the BZ (using the notation of Ref. 36) is reported in Fig. 2 for hafnon and zircon. The band structure is similar for both materials, with valence bands consisting of four well-separated manifolds (labeled with the Roman numbers I–IV starting from the lowest in energy). The typical corresponding Wannier functions are reported in Fig. 3, allowing us to identify the chemical character of the orbitals. The first two manifolds (I and II, consisting of two and six bands, respectively) are associated to one $4s$ and three $4p$ orbitals centered on the two Zr (one $5s$ and three $5p$ for Hf) atoms, respectively. These bands do not show any significant dispersion and, accordingly, the atomic s and p orbitals on the metal atoms are not hybridized. For these two manifolds, the only significant difference between zircon and hafnon is a shift of the Hf s and p bands by about 10 eV down with respect to their Zr analogs.

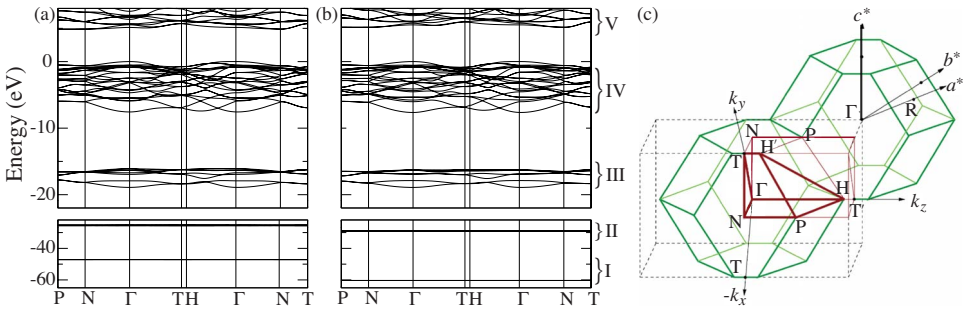

FIG. 2. (Color online) Calculated GW band structure of (a) zircon and (b) hafnon. The corresponding Brillouin zone is illustrated in part (c), adopting the notation of Ref. 36. The various manifolds are labeled with Roman numbers starting from the lowest in energy.

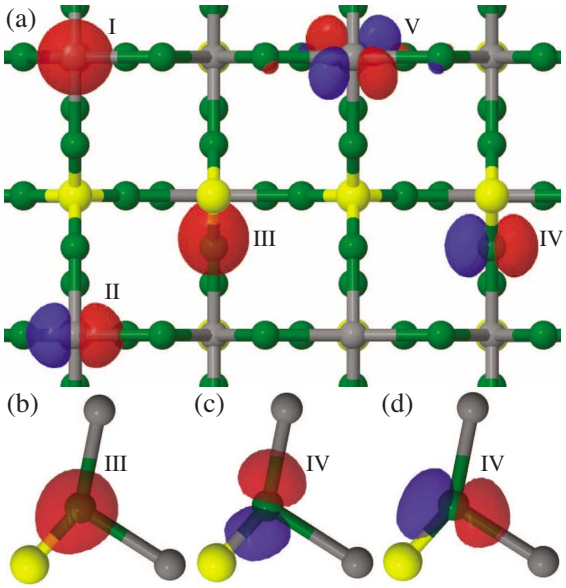

FIG. 3. (Color online) Isosurfaces of the maximally localized Wannier functions for zircon: Red and blue colors indicate opposite isovalues. The O atoms are colored in dark green, Zr atoms in gray, and Si atoms in yellow. The different manifolds are labeled with Roman numbers according to Fig. 2. Different views of the crystal are represented: (a) top view (perpendicular to the tetragonal axis, i.e., the [001] direction) and [(b)–(d)] side view (perpendicular to the [100] or [010] directions, which are equivalent). For the latter, the focus is on an O atom and its three nearest neighbors, two Zr atoms and one Si atom, all lying in the same plane.

The Wannier functions associated to manifold III (consisting of eight bands) show mainly *s* character with their center located close to one of the eight oxygen atoms. In fact, the *s*-like orbital is elongated in the direction of the nearest silicon atoms and its center is shifted accordingly, as illustrated in Fig. 3(b). This indicates a mixing of the O 2*s* orbitals with the Si 3*p* ones. The manifold IV (consisting of 24 bands) covers the last set of valence bands which show the largest dispersion. The corresponding Wannier functions are O 2*p* orbitals with some mixing with Si 3*p* and Zr 4*p* (Hf 5*p*) orbitals, indicating that these electrons are involved in the bonds formation. For each of the eight O atoms, one of the three 2*p*-like orbitals [Fig. 3(a)] is oriented perpendicular to the plane formed by the O atom and its three nearest neighbors, two Zr atoms and one Si atom. This orbital does not show mixing with other atomic orbitals, it corresponds to a lone pair on the O atom. The other two 2*p*-like orbitals [Figs. 3(c) and 3(d)] lie in the plane formed by the O atom and its neighbors and show significant mixing with Si 3*p* and Zr 4*p* (Hf 5*p*) orbitals. The associated electrons are responsible for the bonding. Finally, the Wannier functions associated to manifold V (consisting of the 14 lowest conduction bands) essentially correspond to Zr 4*d* (Hf 5*d*) orbitals with an important mixing with orbitals originating from all the other atoms, as shown in Fig. 3(a).

In Table I, the quasiparticle corrections with respect to the DFT-LDA values are reported for the highest valence band (HVB) and the lowest conduction band (LCB) for both zircon and hafnon. The results computed both within GW_0 and $GW_0\Gamma$ are presented for five high-symmetry **k** points in the BZ. It is worth mentioning that only the P and Γ points correspond to the wavevector grid points for which direct *GW* calculations are performed. For these two points, the calculated quasiparticle corrections and those resulting from the Wannier interpolation differ by less than 0.01 eV. For zircon, the complete band structures, which are obtained using the Wannier interpolation, are presented in Fig. 4.

For both materials, the effect of many-body corrections (see Table I) is to lower the highest valence band and to raise the lowest conduction band. For zircon, the lowering of the HVB ranges from 0.6 to 0.7 eV depending on the **k** point, while the raising of LCB extends between 2.0 and 2.3 eV. For hafnon, the trend is about the same as for zircon. The HVB is lowered by 0.7–0.8 eV, whereas the LCB is shifted up by 1.9–2.4 eV. Moreover, the dispersion of the top valence bands is increased by about 0.6 eV with respect to DFT-LDA [see Fig. 4(a)]. Finally, the valence-band maximum (VBM) location is also affected. In DFT-LDA, the VBM is located at about one tenth of the Γ-*H* symmetry line, away from the Γ point. It is very close in energy with respect to the value at the Γ point. The effect of many-body correc-

TABLE I. Many-body corrections at five high-symmetry **k** points, see Fig. 1(c), for the HVB and the LCB. The many-body corrections are computed within GW_0 and $GW_0\Gamma$ for both zircon and hafnon.

		$ZrSiO_4$			$HfSiO_4$		
k point		LDA	GW_0	$GW_0\Gamma$	LDA	GW_0	$GW_0\Gamma$
Γ	HVB	0.0	−0.7	−0.5	0.0	−0.7	−0.5
	LCB	5.1	+2.1	+2.4	5.5	+1.9	+2.2
P	HVB	−0.5	−0.7	−0.4	−0.5	−0.8	−0.5
	LCB	4.9	+2.0	+2.3	5.2	+2.1	+2.4
N	HVB	−0.7	−0.7	−0.4	−0.6	−0.8	−0.4
	LCB	4.9	+2.0	+2.3	5.2	+2.1	+2.4
T	HVB	−0.8	−0.6	−0.3	−0.9	−0.7	−0.5
	LCB	5.7	+2.2	+2.4	5.9	+2.3	+2.6
H	HVB	−0.7	−0.6	−0.3	−0.8	−0.7	−0.5
	LCB	5.6	+2.3	+2.4	5.9	+2.4	+2.6

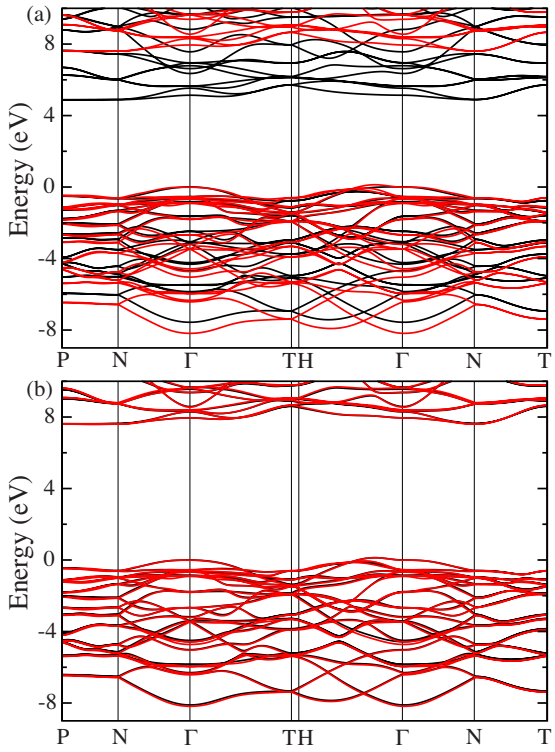

FIG. 4. (Color online) Band structure of zircon: comparison between (a) GW_0 (black) and DFT-LDA (red) (b) GW_0 (black) and $GW_0\Gamma$ (red).

tions [see Fig. 4(a)] is (i) to push the VBM further away from the Γ point at about one-fourth of the Γ-H segment and (ii) to increase the difference in energy between the VBM and the Γ point. Such an effect could not have been identified without resorting to the Wannier interpolation. Note that the many-body corrections do not alter the location of the conduction band minimum.

The calculated quasiparticle gaps are 7.6 and 8.0 eV within GW_0 (7.7 and 8.1 eV within $GW_0\Gamma$) for zircon and hafnon, respectively. These values are much larger than those obtained in DFT-LDA (4.87 for zircon and 5.12 eV for hafnon). They are also significantly larger than the experimental estimations of 6.5–7.0 eV, which are based on measurements on amorphous $(MO_2)_x(SiO_2)_y$ grown on Si.[18–20] Given the differences in the bonding and the coordination numbers between such disordered alloys and the single crystals, such a variation in the gap can be considered as reasonable. Finally, it is worth noting that the calculated quasiparticle gaps are also slightly higher than the values of 7.0 and 7.7 eV obtained for zircon and hafnon, respectively, within DFT-WDA.[10,17] Though WDA is supposed to work better than LDA and GGA approximations, it still suffers from the limitations of DFT calculations.

For both materials, the quasiparticle corrections to the HVB are smaller within GW_0 than within $GW_0\Gamma$. But, at the same time, the corrections to the LCB are larger. The effect of the vertex corrections is thus basically to shift the bands rigidly by 0.3 eV. Thus, once the VBM is set to zero, the GW_0 and $GW_0\Gamma$ band structures can hardly be distinguished, as illustrated in Fig. 4(b) for zircon. This trend has been noticed before for other materials.[21,25]

V. CONCLUSION

The electronic band structure of two high-κ materials, namely, zircon and hafnon, have been investigated within GW and $GW\Gamma$ approximations. The quasiparticle band structure has been calculated using Wannier interpolation scheme. The band structure of both materials is very similar within MBPT and DFT-LDA except for the band gap opening, the increase in the dispersion of the bands, and a slight displacement of the valence-band maximum away from the Γ point within MBPT. On the other hand, both MBPT approximations, GW and $GW\Gamma$, yield almost the same value for the energy gap.

ACKNOWLEDGMENTS

The authors (R.S., M.G., X.G., T.R., and G.-M.R.) acknowledge financial support from the Interuniversity Attraction Poles Program (P6/42)—Belgian State—Belgian Science Policy, the Walloon Region (WALL-ETSF subvention), the Communauté Française de Belgique (Action de Recherche Concertée 07/12-003), the European Union (NMP4-CT-2004–500198) ("NANOQUANTA" Network of Excellence "Nanoscale Quantum Simulations for Nanostructures and Advanced Materials" and "ETSF" Integrated Infrastructure Initiative), and FAME-EMMI Network of Excellence "Functionalized Advanced Materials Engineering."

[1] R. C. Ewing, W. Lutze, and W. J. Weber, J. Mater. Res. **10**, 243 (1995).
[2] J. Robertson, J. Vac. Sci. Technol. B **18**, 1785 (2000).
[3] G. D. Wilk, R. M. Wallace, and J. M. Anthony, J. Appl. Phys. **89**, 5243 (2001).
[4] J. Robertson, Rep. Prog. Phys. **69**, 327 (2006).
[5] R. Puthenkovilakam, E. A. Carter, and J. P. Chang, Phys. Rev. B **69**, 155329 (2004).
[6] J.-P. Crocombette and D. Ghaleb, J. Nucl. Mater. **257**, 282 (1998).
[7] M. Marques, M. Florez, J. M. Recio, L. Gerward, and J. S. Olsen, Phys. Rev. B **74**, 014104 (2006).
[8] J. M. Pruneda, T. D. Archer, and E. Artacho, Phys. Rev. B **70**, 104111 (2004).
[9] J. M. Pruneda and E. Artacho, Phys. Rev. B **71**, 094113 (2005).
[10] K. Xiong, Y. Du, K. Tse, and J. Robertson, J. Appl. Phys. **101**, 024101 (2007).
[11] G.-M. Rignanese, X. Gonze, and A. Pasquarello, Phys. Rev. B **63**, 104305 (2001).
[12] G.-M. Rignanese, X. Gonze, G. Jun, K. Cho, and A. Pasquarello, Phys. Rev. B **69**, 184301 (2004).
[13] S. L. Chaplot, L. Pintschovius, N. Choudhury, and R. Mittal, Phys. Rev. B **73**, 094308 (2006).
[14] J. P. Perdew and M. Levy, Phys. Rev. Lett. **51**, 1884 (1983).

[15] L. J. Sham and M. Schlüter, Phys. Rev. Lett. **51**, 1888 (1983).
[16] G. Onida, L. Reining, and A. Rubio, Rev. Mod. Phys. **74**, 601 (2002).
[17] J. Robertson, K. Xiong, and S. J. Clark, Phys. Status Solidi B **243**, 2054 (2006).
[18] C. Krug and G. Lucovsky, J. Vac. Sci. Technol. A **22**, 1301 (2004).
[19] G. B. Rayner, Jr., D. Kang, Y. Zhang, and G. Lucovsky, J. Vac. Sci. Technol. B **20**, 1748 (2002).
[20] H. Kato, T. Nango, T. Miyagawa, T. Katagiri, K. S. Seol, and Y. Ohki, J. Appl. Phys. **92**, 1106 (2002).
[21] R. Shaltaf, G.-M. Rignanese, X. Gonze, F. Giustino, and A. Pasquarello Phys, Phys. Rev. Lett. **100**, 186401 (2008).
[22] L. Hedin, Phys. Rev. **139**, A796 (1965); L. Hedin and S. Lundqvist, Solid State Phys. **23**, 1 (1969).
[23] M. S. Hybertsen and S. G. Louie, Phys. Rev. B **34**, 5390 (1986).
[24] R. W. Godby, M. Schlüter, and L. J. Sham, Phys. Rev. Lett. **56**, 2415 (1986); Phys. Rev. B **37**, 10159 (1988).
[25] R. Del Sole, L. Reining, and R. W. Godby, Phys. Rev. B **49**, 8024 (1994).
[26] R. W. Godby and R. J. Needs, Phys. Rev. Lett. **62**, 1169 (1989).
[27] N. Marzari and D. Vanderbilt, Phys. Rev. B **56**, 12847 (1997).
[28] J. R. Yates, X. Wang, D. Vanderbilt, and I. Souza, Phys. Rev. B **75**, 195121 (2007).
[29] D. R. Hamann and D. Vanderbilt, Phys. Rev. B **79**, 045109 (2009).
[30] I. Souza, N. Marzari, and D. Vanderbilt, Phys. Rev. B **65**, 035109 (2001).
[31] X. Gonze, J.-M. Beuken, R. Caracas, F. Detraux, M. Fuchs, G.-M. Rignanese, L. Sindic, M. Verstraete, G. Zerah, F. Jollet, M. Torrent, A. Roy, M. Mikami, Ph. Ghosez, J.-Y. Raty, and D. C. Allan, Comput. Mater. Sci. **25**, 478 (2002); X. Gonze, G.-M. Rignanese, M. Verstraete, J.-M. Beuken, Y. Pouillon, R. Caracas, F. Jollet, M. Torrent, G. Zerah, M. Mikami, Ph. Ghosez, M. Veithen, J.-Y. Raty, V. Olevano, F. Bruneval, L. Reining, R. Godby, G. Onida, D. R. Hamann, and D. C. Allan, Z. Kristallogr. **220**, 558 (2005).
[32] M. Teter, Phys. Rev. B **48**, 5031 (1993).
[33] H. J. Monkhorst and J. D. Pack, Phys. Rev. B **13**, 5188 (1976).
[34] S. L. Adler, Phys. Rev. **126**, 413 (1962); N. Wiser, *ibid.* **129**, 62 (1963).
[35] M. Shishkin, M. Marsman, and G. Kresse, Phys. Rev. Lett. **99**, 246403 (2007).
[36] S. Ellialtioglu, E. Mete, R. Shaltaf, K. Allakhverdiev, F. Gashimzade, M. Nizametdinova, and G. Orudzhev, Phys. Rev. B **70**, 195118 (2004).